Intermetallics 100 (2018) 70–76

Contents lists available at ScienceDirect

Intermetallics

journal homepage: www.elsevier.com/locate/intermet

# New insights into perovskite-$Ti_3AlC$ precipitate splitting in a Ti-45Al-5Nb-0.75C alloy by transmission electron microscopy

Li Wang[a,*], Michael Oehring[a], Uwe Lorenz[a], Andreas Stark[a], Florian Pyczak[a,b]

[a] Institute of Materials Research, Helmholtz-Zentrum Geesthacht, Max-Planck-Strasse 1, Geesthacht, D-21502, Germany
[b] Brandenburgische Technische Universität Cottbus-Senftenberg, Konrad-Wachsmann-Allee 17, Cottbus, D-03046, Germany

ARTICLE INFO

*Keywords:*
Intermetallics
Diffusion
Thermal stability
Microstructure
Electron microscopy
Transmission

ABSTRACT

The addition of carbon in TiAl alloys can improve the mechanical properties by precipitate hardening through the perovskite $Ti_3AlC$ carbide. Usually precipitates coarsen during continuous annealing. However, in the Ti-45Al-5Nb-0.75C alloy a splitting of the perovskite carbides was observed in later stages of annealing. By investigation with transmission electron microscopy the details of this splitting process are revealed after annealing at 900 °C. The results show that the re-orientation of the γ phase regions between sub-particles is associated with the splitting step from carbide needles into small sub-particles. γ domains with a different orientation with respect to the γ matrix nucleate and gradually replace the γ matrix phase in regions between the carbide sub-particles. The progress of the splitting process is locally different in different carbides and also in one individual carbide. By increasing the temperature from 800 to 900 °C the growth of the emerging carbide conglomerates and the splitting process of the carbides are greatly accelerated. It is found that both are diffusion-controlled processes.

## 1. Introduction

γ-TiAl alloys have attracted intensive research and emerged as promising high-temperature structural materials due to their excellent mechanical properties (good creep resistance and high strength at elevated temperatures) and light weight [1–4]. The first commercial application of TiAl alloys in aero-engines as low-pressure turbine blades for the GEnx™ engine was introduced by General Electrics [1]. Recently, a β-stabilized TiAl alloy (TNM) has been introduced to the PW 1000G™ engine by Pratt and Whitney [2]. In order to expand the application range towards higher temperatures, γ-TiAl alloys with 5–10 at. % Nb addition have been developed, which show a good balance of properties and excellent oxidation behavior at elevated temperatures [5–7]. Through the addition of carbon, the creep resistance of γ-TiAl alloys is improved due to the precipitation of perovskite carbides [8,9]. The cubic perovskite (P-type) carbide has a similar crystal structure to that of the tetragonal γ-TiAl phase. It can be formed from the $L1_0$ γ-TiAl unit cell by simply replacing the face-centred Al by Ti atoms and putting carbon atoms to the $Ti_6$ octahedral interstices. The stoichiometric formula of P-type carbides is $Ti_3AlC$, but in fact carbon atoms do not fully occupy all interstices [10]. Due to the smaller lattice mismatch between the P-type carbides and the γ phase along the $[001]_\gamma$ orientation compared to the $[100]_\gamma$ and $[010]_\gamma$ directions, P-type carbides grow faster along this direction and appear needle-shaped. With further annealing, they coarsen and remain in a needle-like form until they lose coherency with the γ matrix after extended coarsening [11,12].

For efficient precipitate-strengthening the morphology development and shape stability of the carbides at service temperature are essential in TiAl alloys. Due to the high aspect ratio of the P-$Ti_3AlC$ carbide needles present at the beginning of annealing in TiAl alloys, the precipitates are prone to morphological changes after extended annealing, which can be a significant concern for the long-term creep performance of the alloys. Up to now studies on carbides in TiAl alloys have mainly focused on the ternary Ti-Al-C system [12]. Literature data about the long-term carbide shape development in multinary systems is scarce to non-existent [13–16]. In our previous studies, it was observed for the first time that the carbide precipitates split into smaller sub-particles instead of coarsening after annealing in a Ti-45Al-5Nb-0.75C alloy at 800 °C [17–19]. These studies [17–19] were also the first to the knowledge of the authors in which the splitting of cubic precipitates in a tetragonal matrix has been found. In the present paper, the splitting phenomenon of P-type carbides after annealing at 900 °C is investigated and compared with that at 800 °C in the Ti-45Al-5Nb-0.75C alloy. The carbide splitting process is clarified in detail by conventional (CTEM) and high-resolution transmission electron microscopy (HRTEM). In contrast to our previous work [18], particular emphasis was placed on

* Corresponding author.
*E-mail addresses:* Li.wang1@hzg.de, wlyydy860601@hotmail.com (L. Wang).

https://doi.org/10.1016/j.intermet.2018.06.006
Received 18 April 2018; Received in revised form 29 May 2018
Available online 14 June 2018

the process of the generation of differently oriented γ phase domains between splitting sub-particles and the kinetics and temperature dependence of the splitting process and the carbide conglomerate growth. Such investigations should facilitate to better understand the coarsening kinetics during the splitting process and how newly oriented matrix domains are formed.

## 2. Experimental

The investigated Ti-45Al-5Nb-0.75C (in atomic percent) alloy was produced by a powder metallurgy (PM) route. Pre-alloyed powder was made by plasma melting induction guiding gas atomization (PIGA) and then consolidated using hot-isostatic pressing (HIP) at 1250 °C and 200 MPa for 2 h. The actual carbon content was measured to be 2170 μg/g (0.74 at.%) in the HIPed powder (0–180 μm particle size) using the LECO CS-444 melt extraction system. More detailed information about the material production and the microstructure after HIPing can be found in Refs. [17–20]. In order to form finely dispersed precipitates in the γ matrix, specimens with a size of around $10 \times 10 \times 10\,mm^3$ were first solution-treated at 1250 °C for 5 h, followed by oil quenching and subsequently aged at 800 °C for 336 or 1054 h and at 900 °C for 24, 48 or 96 h. All the heat treatments were performed in air. The microstructures investigated were close to the center of the specimens to avoid possible influences from the surface.

High-energy X-ray diffraction (HEXRD) conducted at the HEMS and HARWI-II beam lines run by the Helmholtz-Zentrum Geesthacht at the Deutsches Elektronen-Synchrotron (DESY) in Hamburg, was used to determine the lattice parameters using Rietveld analysis. The reflections were either recorded with a mar345 image plate or a PerkinElmer XRD 1622 flat panel detector at the HEMS beamline and a mar555 flat panel detector at HARWI-II. The number density, size and morphology of carbides were investigated using a Philips CM200 TEM operated at 200 kV. The size and number density of carbides were determined from TEM images and at least three γ grains were analyzed for each condition. The TEM images were recorded along the $< 100]_\gamma$ and $[001]_\gamma$ lattice directions in order to measure the size along the three dimensions of the carbides and carbide conglomerates. The number density of the precipitates was calculated from the number per unit area divided by the foil thickness. When imaged along the [001] direction the foil thickness could be approximated to be about 100 nm using the convergent-beam electron diffraction technique. The interface between the carbides and the γ matrix, and their atomic arrangement were examined at high resolution using a FEI Titan 80–300 TE M with a $C_s$ image corrector operated at 300 kV. TEM specimens with 2.3 mm diameter were drilled out, mechanically ground to a thickness below 120 μm, and then thinned by twin-jet electro-polishing at 25–35 V and a temperature of −40 °C in a solution of 26 ml perchloric acid (70%), 359 ml 2-butanol and 625 ml methanol. The diffraction patterns of the P-$Ti_3AlC$ carbide and the γ phase were simulated by the software JEMS.

## 3. Results

Fig. 1 shows the simulated diffraction patterns of the P-$Ti_3AlC$ carbide in the < 001 > direction and the γ phase in the [001], [100] and [010] directions as obtained by the JEMS software. In order to make the understanding of the following diffraction investigations easier, the difference in the diffraction patterns between the P-$Ti_3AlC$ carbide and the different orientation variants of the γ phase is discussed in advance. P-type precipitates usually occur with the orientation relationship $[001]_\gamma // < 001 >_P$ and $\{100\}_\gamma // \{100\}_P$. For the P-$Ti_3AlC$ carbide, the diffraction pattern is the same for all three < 001 > directions with existing superlattice reflections {001} and {110}. On the contrary, for the γ phase, the superlattice reflections {110} or (001) appear only in the [001] or [100]/[010] direction, respectively. When the P- < 001 > is pictured parallel with γ-[100] or [010], the reflection $\{001\}_P$ overlaps with $(001)_\gamma$. Thus, in dark-field imaging, both phases appear bright when using this overlapping reflection. But when P- < 001 > is pictured parallel with γ-[001], only the P-$Ti_3AlC$ carbide shows brightness while the γ phase appears dark using the reflection $\{001\}_P$ for dark-field imaging.

Figs. 2–4 illustrate the morphology development of the P-$Ti_3AlC$ carbides by TEM micrographs recorded along the $[100]_\gamma$ and $[001]_\gamma$ orientations in the Ti-45Al-5Nb-0.75C alloy after annealing at 900 °C. All dark-field images were recorded using the diffractions from the P-$Ti_3AlC$ phase and the carbides appear bright. Compared with the situation at 800 °C [18], the process of carbide formation, growth and splitting was significantly accelerated. After annealing for 24 h at 900 °C, carbides have already split and exhibited plate-like configurations. The plate planes of the carbide conglomerates are parallel to either the (100) or (010) crystallographic plane of the γ phase. In the following, details about the re-orientation of the γ phase between the carbide sub-particles during splitting are described. By using dark-field imaging technique, the newly oriented γ phase between sub-particles can be distinguished from the γ matrix and the P-$Ti_3AlC$ phase.

After annealing for 24 h, the diffraction patterns in Fig. 2 showed that the orientation relationship $< 001]_\gamma // < 001 >_P$ and $\{100\}_\gamma // \{100\}_P$ remained between the carbides and the γ matrix. Most carbides at this stage had already split into parallel needles and parts of these needles had further split into smaller carbide sub-particles, as shown in Fig. 2a. Thus, for the needle-like projections of carbide conglomerates, i.e. when viewed along the [100] direction, most of them showed uniform brightness when using $\boldsymbol{g} = 010_P$ and $011_P$ as they were elongated rods of continuous carbide phase. When viewing along the [001] direction, most carbide conglomerates showed the bright cross-section of the needles while the γ matrix between them appeared dark because the used reflections from the P-$Ti_3AlC$ phase were no fundamental or superlattice reflections of the γ matrix. However, for some conglomerates with the former plate plane vertical to the $\boldsymbol{g}$ vector, the γ regions between the sub-particles also showed brightness when using $\boldsymbol{g} = 010_P$ or $100_P$ (schematically shown in the inserts in Fig. 2b). This indicates that these regions have re-oriented by a tilt of 90° relative to the crystallographic orientation of the surrounding matrix phase $\gamma_m$. The 100 or 010 reflection of the newly oriented γ phase in the regions between sub-particles overlaps with the $100_P$ or $010_P$ reflections from the carbide and hence both appear bright. The possible appearance of different types of carbide conglomerates are shown in the inserts in Figs. 2–4. Taking the insert in Fig. 2b as an example a carbide conglomerate with the plate plane being perpendicular to the $\boldsymbol{g}$ vector

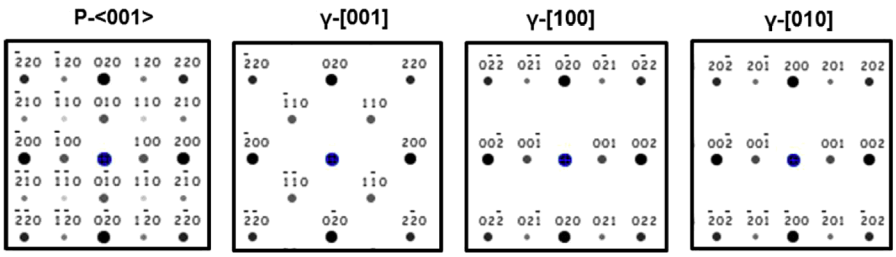


**Fig. 1.** Simulated diffraction patterns of the < 001 > -P-$Ti_3AlC$ carbide and the < 100] and [001] variations of the γ phase by the JEMS program.

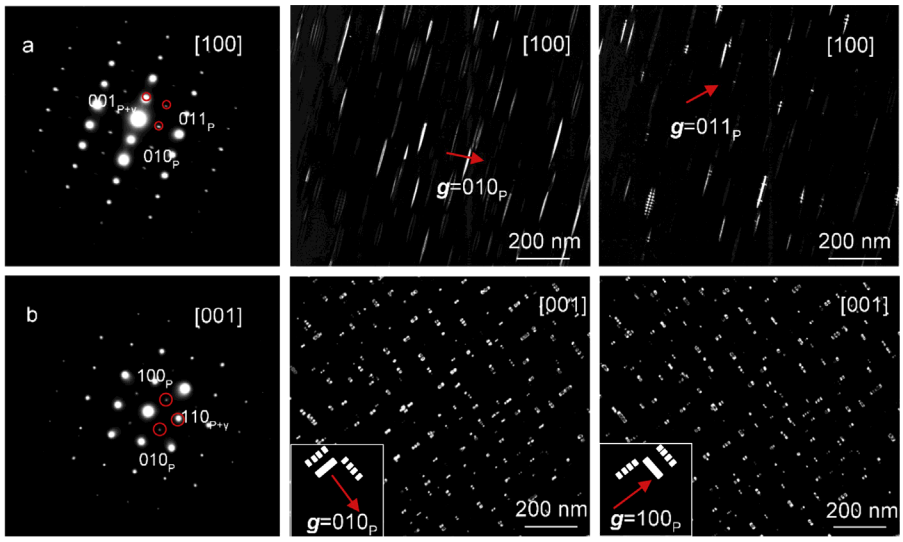


**Fig. 2.** Diffraction patterns of the γ matrix and P-$Ti_3AlC$ carbides, and TEM dark-field micrographs of the P-$Ti_3AlC$ carbides viewed along (a) the [100] direction and (b) the [001] direction in the Ti-45Al-5Nb-0.75C alloy after annealing at 900 °C for 24 h. All dark-field images were recorded in a two-beam condition. The inserts show schematically the contrast of the observed precipitate projections when the reflection indicated in the inserts is used for imaging.

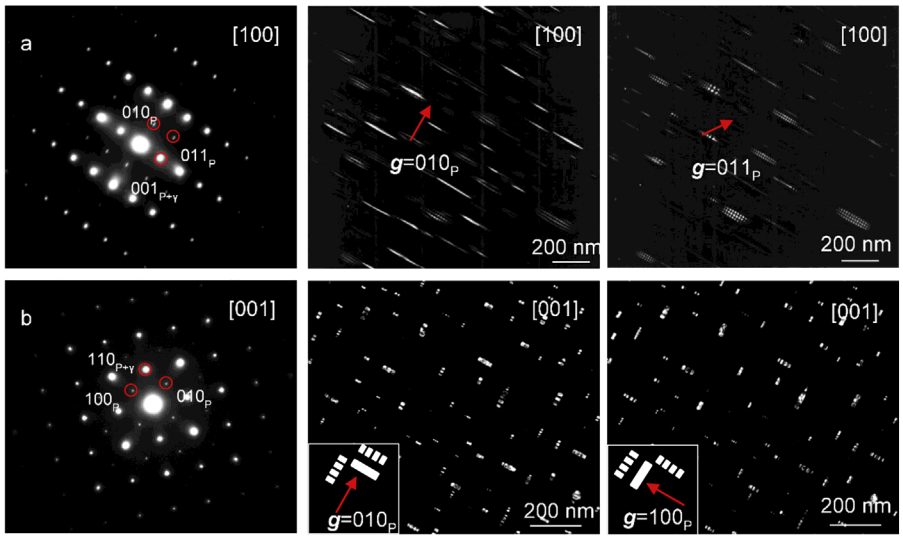


**Fig. 3.** Diffraction patterns of the γ matrix and P-$Ti_3AlC$ carbides, and TEM dark-field micrographs of the P-$Ti_3AlC$ carbides viewed along (a) the [100] direction and (b) the [001] direction in the Ti-45Al-5Nb-0.75C alloy after annealing at 900 °C for 48 h. All dark-field images were recorded in a two-beam condition. The inserts show schematically the contrast of the observed precipitate projections when the reflection indicated in the inserts is used for imaging.

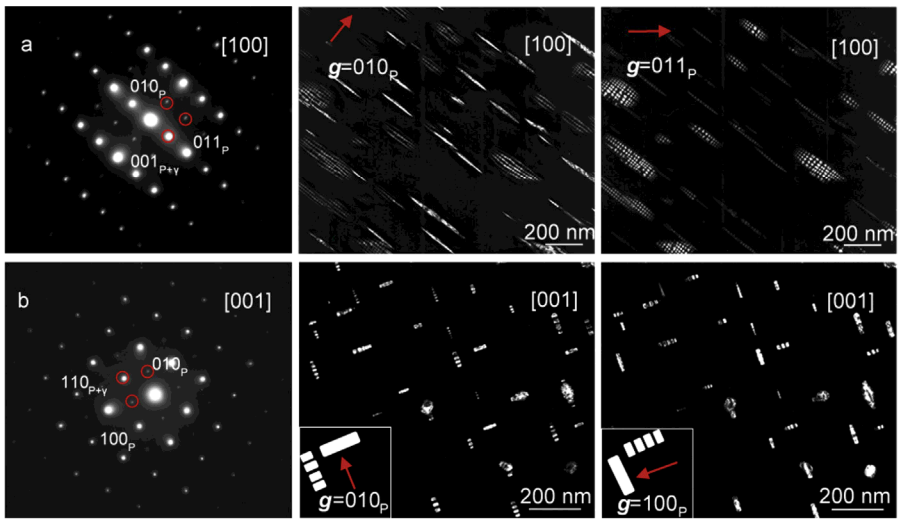


**Fig. 4.** Diffraction patterns of the γ matrix and P-$Ti_3AlC$ carbides, and TEM dark-field micrographs of the P-$Ti_3AlC$ carbides viewed along (a) the [100] direction and (b) the [001] direction in the Ti-45Al-5Nb-0.75C alloy after annealing at 900 °C for 96 h. All dark-field images were recorded in a two-beam condition. The inserts show schematically the contrast of the observed precipitate projections when the reflection indicated in the inserts is used for imaging.

appears either as continuous bright bar or as a row of bright and dark sections. The former is the case when the γ regions between the carbide sub-particles have already re-oriented and the latter when the γ phase between the carbide needles still has the crystallographic orientation of the surrounding γ matrix. Parallel to the $\boldsymbol{g}$ vector the carbide conglomerates always appear as rows of bright and dark sections because irrespective of whether the γ phase between the carbide sub-particles has re-oriented or not it shares no common reflection with the carbide phase for this $\boldsymbol{g}$ vector.

After extended annealing for 48 h, more carbide needles have split into small sub-particles, as shown in Fig. 3a. Viewed along the [100] direction (Fig. 3a), some of the needle-like projections exhibited uniform brightness using both $\boldsymbol{g} = 010_P$ and $011_P$, while the others appeared bright at $\boldsymbol{g} = 010_P$ but showed bright and dark fringes at $\boldsymbol{g} = 011_P$. The latter means that the regions between small sub-particles along the former split needles have also re-oriented. It is interesting to find that when imaged along the [001] direction (Fig. 3b), more regions between the carbide sub-particles appeared bright when using the joint reflections from the carbides and re-oriented γ phase. This suggests that an increasing number of γ phase regions between the sub-particles have changed their orientation or atomic arrangement with increasing annealing time and with more needles splitting into small sub-particles.

After annealing for 96 h (Fig. 4), almost all split needles have further split into small sub-particles. Imaging along the [100] direction, the needle-like projections of the carbide conglomerates showed brightness at $\boldsymbol{g} = 010_P$ and bright and dark fringes at $\boldsymbol{g} = 011_P$. Additionally, when viewed in the [001] direction, now almost all the regions between carbide sub-particles in the carbide conglomerates with former plate plane vertical to the $\boldsymbol{g}$ vector appeared bright when using reflections from the carbides. This means that nearly all the γ phase regions have re-oriented. Based on these results, it is concluded that the re-orientation of the γ phase regions between sub-particles is associated with further splitting carbide needles into small sub-particles.

HRTEM was used to further determine the atomic arrangement of the carbide conglomerates and clarify the splitting process in more details. Fig. 5 shows the cross-sections of the carbide conglomerates at different stages of splitting viewed along the $[001]_\gamma$ direction in the Ti-45Al-5Nb-0.75C alloy after annealing at 900 °C for 24 h. In Fig. 5a, the carbide has started to split into parallel needles via growth of the γ matrix ($\gamma_m$) into the carbide. It should be noted that in the positions indicated by arrows A and B, the atomic arrangement is different. In position A, the γ matrix has completely grown into the carbide and split the carbide, while in position B, the γ matrix only partly intruded in the carbide and a section of the $Ti_3AlC$ carbide lattice structure remained. In Fig. 5b, it is seen that the carbide has split into parallel needles with the γ matrix between the carbide sub-particles. In Fig. 5c the interspersed γ phase ($\gamma_i$) between the parallel needles showed a contrast of

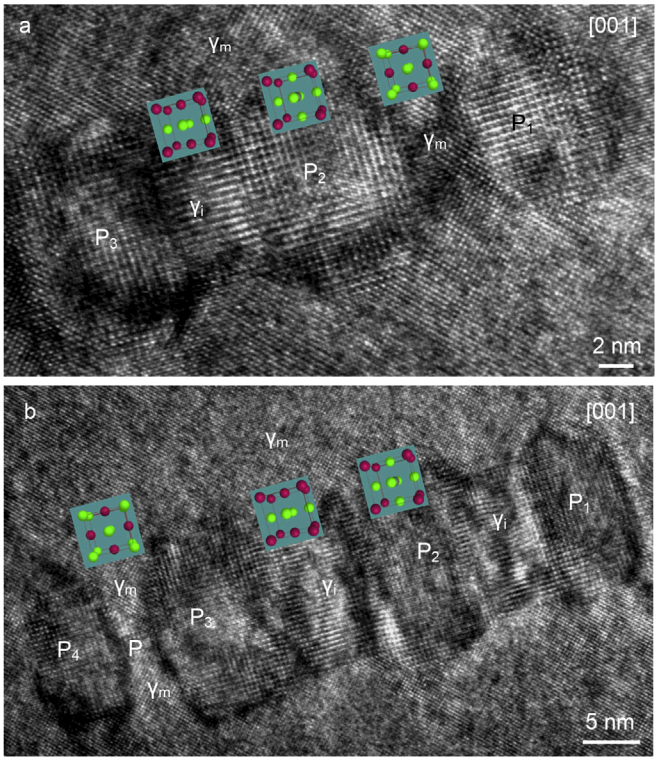


**Fig. 6.** HRTEM images of P-$Ti_3AlC$ carbide conglomerates viewed along the $[001]_\gamma$ direction in the Ti-45Al-5Nb-0.75C alloy after annealing at 900 °C for 48 h (a, b) The γ phase in regions between the split carbide sub-particles has different atomic arrangements ($\gamma_m$ and $\gamma_i$).

alternating darker and brighter atomic planes, which is the atomic arrangement of the γ phase viewed along the [100] or [010] direction. Thus, from these results it is concluded that, firstly, the γ matrix gradually grows into the carbide and splits the carbide into parallel needles. In the second step, these parallel needles split further into smaller sub-particles, meanwhile $\gamma_i$ forms to replace $\gamma_m$ in the regions between sub-particles. Its crystallographic orientation deviates from the γ matrix by 90°.

It is interesting to find that the γ phase had different atomic arrangements in the regions between the split carbide needles, as shown in Fig. 6. Here the cross-sections of the carbide conglomerates are imaged along the $[001]_\gamma$ direction in the Ti-45Al-5Nb-0.75C alloy after annealing at 900 °C for 48 h. In Fig. 6a the atomic arrangement in the region between $P_1$ and $P_2$ remained the same as in the γ matrix if

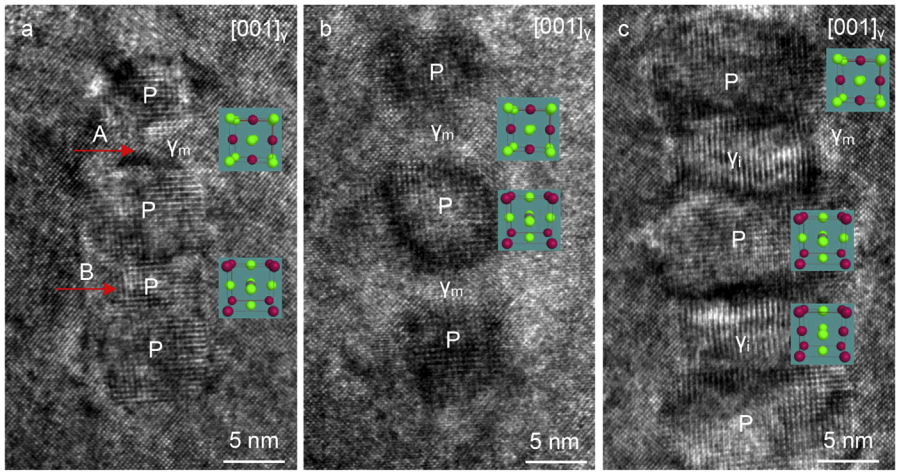


**Fig. 5.** HRTEM images of the P-$Ti_3AlC$ carbide conglomerates viewed along the $[001]_\gamma$ direction in the Ti-45Al-5Nb-0.75C alloy after annealing at 900 °C for 24 h. (a) Carbide splitting starts via the growth of the γ matrix into the carbide, (b) the carbide has split into three parallel needles with the γ matrix in between and (c) the orientation of the γ phase between the split carbides has changed.

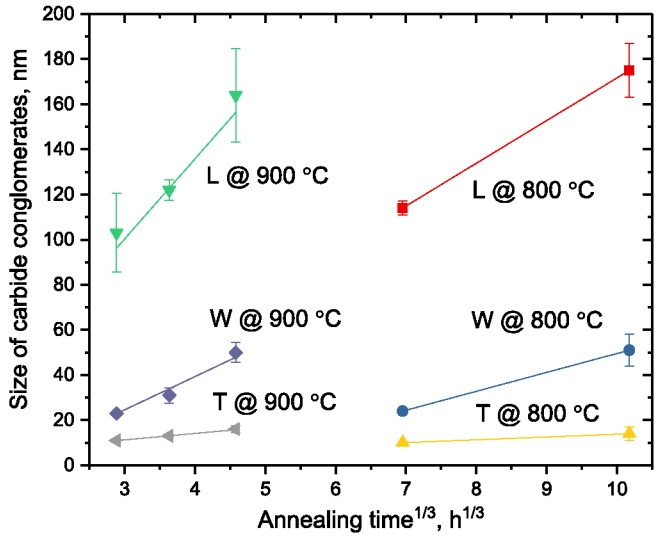


**Fig. 7.** (A) Size and (b) number density of the carbide conglomerate as a function of annealing temperature and time (with standard deviation bars) in the Ti-45Al-5Nb-0.75C alloy. L: length, W: width and T: thickness.

viewed along the $[001]_\gamma$ direction. But $\gamma_i$ between $P_2$ and $P_3$ had the atomic arrangement as if imaged along the $[100]_\gamma$ or $[010]_\gamma$ direction. This configuration of the carbide conglomerate represents different states of ingrowth and re-orientation of the regions between the carbide sub-particles during splitting into small sub-particles. In Fig. 6b, $\gamma_i$ had already formed in the regions between $P_1$ and $P_2$ as well as $P_2$ and $P_3$. But the region between $P_3$ and $P_4$ still had the $\gamma$ matrix lattice orientation together with a remaining section of the P-phase lattice in the middle. These results suggest that the splitting process within one individual carbide precipitate could be locally different.

Fig. 7 displays the size and number density of the carbide conglomerates as a function of annealing temperature and time. It can be recognized that the growth along the length direction ([001]) is faster than along the width and thickness directions ([100] and [010]). This may be due to a lower lattice misfit and resulting lower coherency stresses and also to a smaller elastic modulus along the [001] direction of the $\gamma$ matrix [18]. After annealing at 800 °C for 336 h, the carbide conglomerates have an average size of length (L) = 114 ( ± 3) nm, width (W) = 24 ( ± 1) nm, and thickness (T) = 10 ( ± 1) nm and a number density of 0.24 ( ± 0.02) × $10^{22}$/m$^3$. With extended annealing for 1054 h, the conglomerate size increases to L = 175 ( ± 12) nm, W = 51 ( ± 7) nm, and T = 14 ( ± 3) nm, while the number density decreases to 0.08 ( ± 0.01) × $10^{22}$/m$^3$. Increasing the temperature to 900 °C, the carbide conglomerates have reached an average size of L = 103 ( ± 17) nm, W = 23 ( ± 1) nm, and T = 11 ( ± 1) nm and a number density of 0.27 ( ± 0.07) × $10^{22}$/m$^3$ after annealing for 24 h, which are very similar to those at 800 °C for 336 h. With further annealing for 48 h at 900 °C, the carbide conglomerates grew (L = 122 ( ± 5) nm, W = 31 ( ± 3) nm, and T = 13 ( ± 1) nm) and the number density decreased obviously (around 0.09 ( ± 0.01) × $10^{22}$/m$^3$). A further increase in the size of carbide conglomerates (L = 164 ( ± 21) nm, W = 50 ( ± 4) nm, and T = 16 ( ± 2) nm) and decrease in the number density (around 0.04 ( ± 0.01) × $10^{22}$/m$^3$) was observed after annealing for 96 h. The conglomerate size is close to that after annealing for 1054 h at 800 °C, while the density is only half of the value determined at 800 °C for 1054 h.

## 4. Discussion

It has been discussed in our previous publication [18] that carbide splitting in TiAl alloys during annealing could be energetically favorable owing to the elastic interaction energy between the split sub-particles. As predicted by theoretical calculation in literature [21–24], the elastic interaction energy can be negative and leads to an energy reduction when the particles are aligned along the elastically soft directions of an elastically anisotropic matrix phase. In Ni-base superalloys, the splitting of $\gamma'$ precipitates was observed but it was still a matter of debate how the splitting started [25]. Some researchers thought that the splitting process was initiated by the amplification of perturbations along the precipitate-matrix interface [26,27]. But others proposed that it was started via the formation of the matrix phase in the center of the precipitate [23]. In the present study for the very similar process of splitting in $\gamma$-TiAl alloys this can be unambiguously decided. It is clearly observed that the $\gamma$ matrix gradually grows into the carbide precipitates to split them into parallel needles which further decompose into smaller sub-particles. So, for the case of carbides in TiAl alloys an initiation of the splitting process at the center of the precipitates can be ruled out and splitting is most probably initiated at perturbations of the precipitate-matrix interface. During the decomposition of the parallel carbide needles into sub-particles the atomic arrangement of the $\gamma$ phase between the carbide sub-particles gradually changes from $\gamma_m$ to $\gamma_i$. After the first splitting step, carbide needles aligned along the c-axis of the $\gamma$ matrix resulted. The $\gamma$ phase in the regions between carbide needles still preferred the same orientation as the $\gamma$ matrix. However, when the carbide needles further split into smaller sub-particles the interspersed matrix changed the orientation of the c-axis by 90°, which results in a reduction of the elastic strain energy between $\gamma_i$ and the sub-particles due to the tetragonality of the $\gamma$ phase. Since an interface between the $\gamma_i$ and $\gamma$ matrix is created in this process, a nucleation barrier has to be overcome. Nucleation could take place in the $\gamma$ matrix at the interface to the carbide sub-particles where the coherency stresses are largest. This would require only short-range diffusion processes in which atoms on the (001) face-centred sites are exchanged by those on (100) or (010) face-centred sites. The result would be a so-called 120° rotational domain which has the same stacking sequence of the close-packed planes as the matrix phase but an orthogonal c-axis. Such domains often occur in lamellar microstructures [28]. These domains could then grow and fill the space between the carbide sub-particles. Alternatively, nucleation could also occur in the carbide particles as has been observed for Ni-base superalloys [23,29]. In this case C and Ti would have to diffuse out of and Al and Nb into the carbides besides short-range diffusion processes and nucleation thus appears to be kinetically hindered. Since furthermore in the present work matrix particles inside carbides have never been observed it is concluded that $\gamma_i$ is nucleated in the matrix.

As reported in Ref. [18], the $\gamma_i$ region between the split sub particles has a very similar Ti, Al and Nb content but a much higher C concentration compared with $\gamma_m$. The increased C concentration in the $\gamma_i$ domains between the carbide sub-particles might be due to a non-equilibrium state. This would be surprising because the specimens have been annealed for over 1000 h which should have provided sufficient time to achieve equilibrium via diffusion processes. The increased C concentration could also be attributed to the elastic strain field caused by the carbide precipitates. It is reported in literature [30,31] that the elastic strain field affected the equilibrium solute distribution in the vicinity of elastically interacting precipitates and net solute segregation was observed in the matrix surrounding the interacting particles.

It is clearly seen in Fig. 7 that the carbide conglomerates grow with increasing annealing time. In the following it is assumed that nearly the maximum volume fraction of carbides has been precipitated for the annealing times shown in Fig. 7a, i.e. the supersaturation of C has almost been exhausted. At least for annealing 1054 h at 800 °C this can be concluded from the mentioned atom probe results published in Ref. [18] which showed that the C content in the matrix is similar to the C solubility. It also agrees with HEXRD measurements of the carbide volume fraction, which only show a slight increase after annealing for 1054 h [32]. From the density evolution of the carbide conglomerates in Fig. 7b it is shown that the number density decreases with increasing

annealing time. This indicates that even in the annealing stage in which splitting occurs, growth via Ostwald ripening (bigger carbide conglomerates consuming smaller ones) exists. Nevertheless, coarsening slows down after extended annealing. Additionally, due to calculations for a Ni-base superalloy, the elastic interaction energy is most favorable when the split particles are separated by a distance of 1.09D (D is the particle diameter) in the < 100 > directions [22,23]. Thus, it is speculated that the distance between the split particles ($\gamma_i$ region) will assume an optimum value relative to the size of the sub-particles. In this case a conglomerate of carbides then can grow by a combined growth of the split sub-carbides and the $\gamma_i$ region between the sub-particles. At temperatures below 1200 °C the diffusion coefficients of the major elements, Ti and Al, follow the Arrhenius law $D = D_0 \exp(-Q/RT)$. The Arrhenius parameters are reported to be $D_0 = 1.43 \times 10^{-6}\,m^2/s$, $Q = 2.59$ eV $(249.90 \times 10^3$ J/mol) and $D_0 = 2.11 \times 10^{-2}\,m^2/s$, $Q = 3.71$ eV $(357.96 \times 10^3$ J/mol) for Ti and Al, respectively in TiAl [33]. $R$ is the gas constant (8.314 J/mol). By using the values mentioned above, the diffusion coefficients of Ti and Al at 800 and 900 °C are calculated to be $D_{\text{Ti-800 °C}} = 9.89 \times 10^{-19}\,m^2/s$, $D_{\text{Ti-900 °C}} = 1.09 \times 10^{-17}\,m^2/s$, $D_{\text{Al-800 °C}} = 8.11 \times 10^{-20}\,m^2/s$ and $D_{\text{Al-900 °C}} = 2.43 \times 10^{-18}\,m^2/s$. This means if the temperature increases from 800 to 900 °C, the diffusion coefficient of Ti is increased by around 11 times and that of Al by about 30 times. Assuming the Lifshitz-Slyozov-Wagner (LSW) law for coarsening [25,34,35], the particle radius of precipitates, $R$, is proportional to $\sqrt[3]{a_{LSW}\,t}$, where $t$ is the annealing time and $\alpha_{LSW}$ the LSW constant which is proportional to the diffusion coefficient $D$. In Fig. 7a the length, width and thickness of the carbide conglomerates is plotted against $t^{1/3}$, which shows a linear development with $t^{1/3}$. By comparing the slopes of these lines at 800 and 900 °C, it is found that $D_{900\,°C}/D_{800\,°C}$ is around 10 which agrees quite well with what would be expected using the above given diffusion coefficients of Ti in TiAl at 800 and 900 °C. Furthermore, it is found that a higher temperature leads to a faster carbide splitting. It starts after 168 h annealing at 800 °C, while carbides split much earlier at 900 °C. Thus, from these results it is concluded that the growth of the carbide conglomerates and the splitting process are diffusion-controlled processes driven by strain energy and the kinetics is accelerated due to a faster atomic diffusion at a higher temperature. A contribution of the precipitate interface-mobility to the coarsening kinetics, which might have been suspected due to the high aspect ratio of the precipitates, is not indicated by the results. However, other factors, such as the temperature dependence of misfit and elastic modulus may also influence the splitting process. It was determined by HEXRD that the lattice parameters of the phases ($a_\gamma = 4.02$ Å, $c_\gamma = 4.07$ Å and $a_P = 4.15$ Å) are nearly the same at 800 and 900 °C, which results in a similar lattice misfit. The elastic modulus of the γ matrix does not change significantly based on the data in a single crystal γ-TiAl alloy [36]. Thus, effects from these two factors could be ruled out.

## 5. Conclusions

In this study, the splitting process of the perovskite carbides after annealing for different temperatures and times was investigated in detail in a Ti-45Al-5Nb-0.75C alloy. It has been clearly observed that the γ matrix gradually grows into the carbide precipitates to split them into parallel needles which further decompose into smaller sub-particles. An initiation of the splitting process at the center of the precipitates can be ruled out and splitting is most probably initiated at perturbations of the precipitate-matrix interface. It is found that the reorientation of the γ phase in the regions between the carbide sub-particles is associated with the splitting step from carbide needles into small sub-particles. This process most probably occurs by $\gamma_i$ nucleation in the matrix phase at the interface to the carbide sub-particles and results in a reduction of the elastic strain energy between these regions and the sub-particles due to the tetragonality of the γ phase. It is interesting that the reorientation of the γ phase does not happen simultaneously between all sub-particles, even in one individual carbide conglomerate. By comparing the kinetics with the temperature dependence of diffusion it is concluded that the conglomerate growth and the splitting process are diffusion-controlled.

## Acknowledgements

The authors are grateful to Dr. Frank-Peter Schimansky and Dirk Matthiessen for producing the HIPed pre-alloyed powder. Li Wang acknowledges the Helmholtz Association for funding her Postdoc project at Helmholtz-Zentrum Geesthacht in the framework of the Helmholtz Postdoc program. The support from the National Natural Science Foundation of China (No. 51401241) is acknowledged.

## References

[1] B.P. Bewlay, M. Weimer, T. Kelly, A. Suzuki, P.R. Subramanian, The science, technology, and implementation of TiAl alloys in commercial aircraft engines, in: I. Baker, M. Heilmaier, S. Kumar, K. Yoshimi (Eds.), Intermetallic-Based Alloys-Science, Technology and Applications, Materials Research Society Symp. Proc. vol. 1516, Cambridge University Press, Cambridge, UK, 2013, pp. 49–58.
[2] U. Habel, F. Heutling, D. Helm, C. Kunze, W. Smarsly, G. Das, H. Clemens, Forged intermetallic-TiAl based alloy low pressure turbine blade in the geared turbofan, in: V. Venkatesh, A.L Pilchak, J.E. Allison, S. Ankem, R. Boyer, J. Christodoulou, H.L. Fraser, M. Ashraf Imam, Y. Kosaka, H.J. Rack, A. Chatterjee, A. Woodfield (Eds.), Proceedings of the 13th World Conference on Titanium, San Diego, CA, USA, vol. 2015, John Wiley & Sons, Inc, Hoboken, NJ, USA, 2016, pp. 1223–1227.
[3] F. Appel, M. Oehring, R. Wagner, Novel design concepts for gamma-base titanium aluminide alloys, Intermetallics 8 (2000) 1283–1312.
[4] F. Appel, J.D.H. Paul, M. Oehring, Gamma Titanium Aluminide Alloys: Science and Technology, Wiley-VCH, Weinheim, Germany, 2011.
[5] M. Yoshihara, K. Miura, Effects of Nb addition on oxidation behavior of TiAl, Intermetallics 3 (1995) 357–363.
[6] S. Taniguchi, K. Uesaki, Y.C. Zhu, H.X. Zhang, T. Shibata, Influence of niobium ion implantation on the oxidation behaviour of TiAl under thermal cycle conditions, Mater. Sci. Eng. A 249 (1998) 223–232.
[7] W.J. Zhang, S.C. Deevi, G.L. Chen, On the origin of superior high strength of Ti-45Al-10Nb alloys, Intermetallics 10 (2002) 403–406.
[8] M. Nemoto, W.H. Tian, K. Harada, C.S. Han, T. Sano, Microstructure of precipitation strengthened $Ni_3Al$ and TiAl, Mater. Sci. Eng. A 152 (1992) 247–252.
[9] U. Christoph, F. Appel, R. Wagner, Dislocation dynamics in carbon-doped titanium aluminide alloys, Mater. Sci. Eng. A 239–240 (1997) 39–45.
[10] M.A. Pietzka, J.C. Schuster, Summary of constitutional data on the Aluminum-Carbon-Titanium system, J. Phase Equil. 15 (1994) 392–400.
[11] S. Chen, P.A. Beaven, R. Wagner, Carbide precipitation in γ-TiAl alloys, Scripta Metall. Mater. 26 (1992) 1205–1210.
[12] W.H. Tian, T. Sano, M. Nemoto, Structure of perovskite carbide and nitride precipitates in $L1_0$-ordered TiAl, Philos. Mag. A 68 (1993) 965–976.
[13] Y. Wu, Y.W. Park, H.S. Park, S.K. Hwang, Microstructural development of indirect-extruded TiAl-Mn-Mo-C intermetallic alloys during aging, Mater. Sci. Eng. A 347 (2003) 171–179.
[14] R.J. Simpkins II, M.P. Rourke, T.R. Bieler, P.A. McQuay, The effects of HIP pore closure and age hardening on primary creep and tensile property variations in a TiAl XD(TM) alloy with 0.1 wt.% carbon, Mater. Sci. Eng. A 463 (2007) 208–215.
[15] P.A. McQuay, R. Simpkins, D.Y. Seo, T.R. Bishop, Alloy and process improvements for cast TiAl alloy applications, in: Y.W. Kim, D.M. Dimiduk, M.H. Loretto (Eds.), Gamma Titanium Aluminides TMS, San Diego, California, 1999, pp. 197–207.
[16] H.S. Park, S.K. Hwang, C.M. Lee, Y.C. Yoo, S.W. Nam, N.J. Kim, Microstructural refinement and mechanical properties improvement of elemental powder metallurgy processed Ti-46.6Al-1.4Mn-2Mo alloy by carbon addition, Metall. Mater. Trans. 32 (2001) 251–259.
[17] L. Wang, H. Gabrisch, U. Lorenz, F.P. Schimansky, A. Stark, F. Pyczak, Perovskite $Ti_3AlC$ carbide splitting in high Nb containing TiAl alloys, Mater. Res. Soc. Symp. Proc. 1760 (2015) 31–36.
[18] L. Wang, C. Zenk, A. Stark, P. Felfer, H. Gabrisch, M. Göken, U. Lorenz, F. Pyczak, Morphology evolution of $Ti_3AlC$ carbide precipitates in high Nb containing TiAl alloys, Acta Mater. 137 (2017) 36–44.
[19] L. Wang, U. Lorenz, M. Münch, A. Stark, F. Pyczak, Influence of alloy composition and thermal history on carbide precipitation in γ-based TiAl alloys, Intermetallics 89 (2017) 32–39.
[20] D. Laipple, L. Wang, M. Rackel, A. Stark, B. Schwebke, A. Schreyer, F. Pyczak, Microstructure of gas atomised γ-TiAl based alloy powders, MRS Adv. (2017) 1–6, http://dx.doi.org/10.1557/adv.2017.88.
[21] W. Johnson, J.K. Lee, Elastic interaction energy of two spherical precipitates in an anisotropic matrix, Metall. Trans. A 10 (1979) 1141–1149.
[22] T. Miyazaki, H. Imamura, H. Mori, T. Kozakal, Theoretical and experimental investigations on elastic interactions between γ'-precipitates in a Ni-Al alloy, J. Mater. Sci. 16 (1981) 1197–1203.
[23] T. Miyazaki, H. Imamura, T. Kozakai, The formation of "γ' precipitate doublets" in Ni-Al alloys and their energetic stability, Mater. Sci. Eng. 54 (1982) 9–15.
[24] M. Doi, T. Miyazaki, T. Wakatsuki, The effect of elastic interaction energy on the

morphology of γ' precipitate in Ni-based alloys, Mater. Sci. Eng. 67 (1984) 247–253.
[25] R. Wagner, R. Kampmann, P.W. Voorhees, Homogeneous second-phase precipitation, in: G. Kostorz (Ed.), Phase Transformations in Materials, Wiley-VCH Verlag GmbH & Co. KGaA, Weinheim, Germany, 2005, pp. 309–407.
[26] M.J. Kaufman, P.W. Voorhees, W.C. Johnson, F.S. Biancaniello, An elastically induced morphological instability of a misfitting precipitate, Metall Trans A 20 (1989) 2171–2175.
[27] Y.S. Yoo, D.Y. Yoon, M.F. Henry, The effect of elastic misfit strain on the morphological evolution of γ'-precipitates in a model Ni-base superalloy, Met. Mater. 1 (1995) 47–61.
[28] S. Zghal, S. Naka, A. Couret, A quantitative TEM analysis of the lamellar microstructure in TiAl based alloys, Acta Mater. 45 (1997) 3005–3015.
[29] F. Vogel, N. Wanderka, Z. Balogh, M. Ibrahim, P. Stender, G. Schmitz, J. Banhart, Mapping the evolution of hierarchical microstructures in a Ni-based superalloy, Nat. Commun. 4 (2013) 2955, http://dx.doi.org/10.1038/ncomms3955.
[30] W.C. Johnson, P.W. Voorhees, Equilibrium solute concentration surrounding elastically interacting precipitates, Metall. Trans. A 16A (1985) 337–347.
[31] K.C. King, P.W. Voorhees, G.B. Olson, T. Mura, Solute distribution around a coherent precipitate in a multicomponent alloy, Metall. Trans. A 22 (1991) 2199–2210.
[32] L. Wang, H. Gabrisch, U. Lorenz, F.P. Schimansky, A. Schreyer, A. Stark, F. Pyczak, Nucleation and thermal stability of carbide precipitates in high Nb containing TiAl alloys, Intermetallics 66 (2015) 111–119.
[33] Y. Mishin, Chr. Herzig, Diffusion in the Ti-Al system, Acta Mater. 48 (2000) 589–623.
[34] I.M. Lifshitz, V.V. Slyozov, The kinetics of precipitation from supersaturated solid solutions, J. Phys. Chem. Solid. 19 (1) (1961) 35–50.
[35] C. Wagner, Theorie der Alterung von Niederschlägen durch Umlösen (Ostwald-Reifung), Z Elektroch (Ber. Bunsenges. Phys. Chemie) 65 (1961) 581–591.
[36] Y. He, R.B. Schwarz, T. Darling, M. Hundley, S.H. Whang, Z.M. Wang, Elastic constants and thermal expansion of single crystal γ-TiAl from 300 to 750 K, Mater. Sci. Eng. A 239–240 (1997) 157–163.